Light Management for Enhancing Optical Gain in a Solar-Pumped Fiber Laser Employing a Solid-State Luminescent Solar Concentrator

Taizo Masuda,* Kai Aoyagi, Stephan Dottermusch, Ian A. Howard, Bryce S. Richards, and Masamori Endo

Optical gain of 8.3 km^{-1} is obtained in a neodymium-doped silica fiber under simulated sunlight (intensity = 2.1 kW m^{-2}). The fiber gain medium (length = 50 m) is coiled and attached to a solid-state luminescent solar concentrator (LSC) disk (diameter = 180 mm). The disk/fiber unit is placed in a cavity comprising highly reflective (HRM) and dichroic (DM) mirrors to increase the photon confinement by a factor of 2.2 compared with a liquid LSC (also employing HRM/DM). The enhancement is mainly due to the air gap between HRM/DM and LSC, which affords total internal reflection (TIR) in the solid-state LSC and an ideal boundary condition for the multilayer mirrors. The numerical calculations indicate that an additional 2.2-times enhancement is achievable with a side wall exhibiting 90% diffuse reflection. This has been experimentally confirmed (1.9-times optical-gain enhancement is realized by adding a polytetrafluoroethylene side-wall reflector). Overall, the solid-state LSC-based solar-pumped laser (SPL) comprising reflective side walls exhibits a gain factor of 4.2, which is superior to its liquid-state predecessor. Further improvements employing a solid-state LSC design and fiber optimization will facilitate the market penetration of SPLs.

1. Introduction

The direct conversion of broadband solar radiation into highly coherent laser radiation has attracted scientific and practical interest in recent years.[1] After the first demonstration of a solar-pumped laser (SPL) in 1963,[2] subsequent studies were focused on improving the laser medium and the solar collector design, thereby achieving state-of-the-art high-power SPLs with solar collecting efficiency of up to 32.5 W m^{-2} (laser output power per unit area of the solar collector optics).[3,4] Such state-of-the-art SPLs comprised laser media, such as Nd^{3+}-doped single-crystal yttrium aluminum garnet (Y$_3$Al$_5$O$_{12}$) rods, which were pumped by concentrated sunlight (the concentration factors were in the order of thousands).[5–9]

SPLs exhibit many potential applications, including solar hydrogen generation, photovoltaic energy conversion, space solar power systems, space propulsion, and remote area telecommunications.[1,10–17] In addition, SPLs with 20 kW output powers could be achieved by exploiting megawatt-scale solar furnaces; these SPLs could be employed in a fossil-fuel-free energy cycle in which magnesium is chemical energy storage for sunlight.[1,18–20] Despite the range of potential applications, the utilization of highly concentrated sunlight has severely restricted the practical applications of SPLs owing to their dependence on an accurate solar tracking system.[21] Further, only the direct components of sunlight can be harvested by concentrating optical elements, such as lenses or mirrors; they do not function efficiently under cloudy conditions when the diffuse component of sunlight is high. Regarding locations, including Susono (Japan) and Karlsruhe (Germany), diffuse horizontal solar radiation represents ≈49% of the total terrestrial sunlight averagely received annually.[22] Furthermore, removing the reliance of SPLs on concentrating optics would further render the technology comparable with that of photovoltaic panels, thus availing new applications for SPLs since the modularity of such flat-plate devices would also favor small-scale applications.[23–25]

Although SPLs, which do not require a mirror/lens-based concentrator system, have been studied for a long time since their introduction in 1983,[26] the technology was only demonstrated

T. Masuda
Carbon Neutral development division
Toyota Motor Corporation
410-1193 Susono, Shizuoka, Japan
E-mail: taizo_masuda@mail.toyota.co.jp

T. Masuda
Institute for Advanced Science
The University of Electro-Communications
182-8585 Chofu, Tokyo, Japan

K. Aoyagi, M. Endo
Department of Physics
Tokai University
259-1292 Hiratsuka, Kanagawa, Japan

S. Dottermusch, I. A. Howard, B. S. Richards
Institute of Microstructure Technology
Karlsruhe Institute of Technology
76344 Eggenstein-Leopoldshafen, Germany

recently. In 2020, Masuda et al. demonstrated a fully planar SPL that is based on a fiber laser with transverse excitation geometry in which sunlight was spectrally concentrated via radiative energy transfer from a luminescent dye in solution, thus removing any requirement for lenses or mirrors.[27] In the system, an Nd^{3+}-doped active silica fiber (length = 190 m) was utilized as the active medium, which was coiled into a ring and enclosed in a shallow cylindrical container (diameter = 300 mm), which also contained a sensitizer solution. The lid of this container was a dichroic mirror (DM) that was designed to exhibit a transmission cutoff wavelength of 570 nm, while the bottom surface and side wall were coated with a highly reflective dielectric mirror (HRM), thus obtaining a liquid-state luminescent solar concentrator (LSC). The LSC confine the down-shifted photons by the sensitizer until they were absorbed by the Nd^{3+} ions. This laser system could utilize direct and diffuse sunlight for lasing; moreover, it required an extremely low solar flux (700 W m^{-2} (0.7 suns)) front-side illumination at the top of its window. Lasing was achieved under terrestrial sunlight (maximum power output = 1.3 mW with an optical gain of 2.1 km^{-1}).[27]

After demonstrating the planar SPL, the theoretical investigations indicated that a 7-fold enhancement of the optical gain, which would achieve a 30-fold enhancement of the laser output power, could be realized by substituting the liquid-state LSC with a solid-state one (maintaining the diameter (300 mm) of the LSC and the fiber length (190 m)).[28] Such a significant improvement is attributable to the application of total internal reflection (TIR) in the solid-state LSC. TIR was unachievable in the original liquid-state LSC since light transport relied solely on the reflectance of DM/HRM. These mirrors consist of multiple dielectric layers and invariably exhibit sub-unity reflectance, especially for the *p*-polarized, obliquely incident light. This dichroic stack design cannot function efficiently when the refractive index (*n*) of the LSC medium (methanol) is close to those of the dielectric materials comprising the mirrors (SiO_2 or TiO_2).[29] Even the reflectivity of the *p*-polarized light in our best-performing "hot-mirror" at incident angles of >50° was <80% inside the LSC.

Inspired by the theoretical results,[28] a proof-of-concept planar SPL system was fabricated employ a solid-state LSC. Here, we experimentally demonstrated an optical gain of 8.3 km^{-1} in this proof-of-concept SPL under xenon-lamp irradiation (intensity = 2.1 kW m^{-2}). The gain of the solid-state LSC normalized to LSC area and absorbed excitation power exceeds that achieved in the liquid-phase counterpart by more than a factor of three.[28] The enhancement of the gains corresponded well with the results of numerical simulations.

2. Experimental Section

2.1. Fabrication of LSC

Figure 1 depicts a schematic and photo of the fabricated prototype planar SPL, which was based on a thin-film solid-state LSC comprising a fluoropolymer film (thickness = 30 μm) containing the fluorescent organic dyes. The SPL is a fiber laser with transverse excitation geometry that is pumped with the downshifted photons produced by the dye in the LSC. The film was coated onto a fused silica (SiO_2) substrate (diameter = 180 mm). The
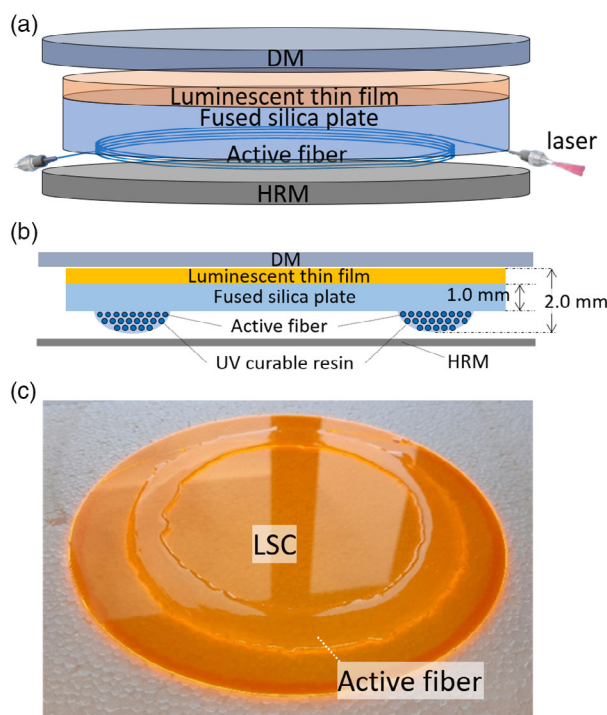

Figure 1. a) Schematic representation of the fabricated prototype SPL employing a thin-film solid-state LSC. b) Schematic representation of the cross-section of the prototype SPL. c) Photograph of the underside of the fabricated prototype SPL without DM and HRM.

thin luminescent layer comprised Lumogen F Orange 240 (O240, 5000 ppm), a perylene dye, whose emission peak at ≈590 nm exhibited an excellent overlap with the $^{4}G_{5/2}$–$^{2}G_{7/2}$ transitions of Nd^{3+} absorption (**Figure 2**).[28] Further, Lumogen F Yellow 083 (Y083) was added as a second dye to boost the absorption in the blue region (<450 nm) to exploit its fluorescence via cascade energy transfer. The fabrication procedure of the thin-film solid-state LSC is described in the Supporting information.
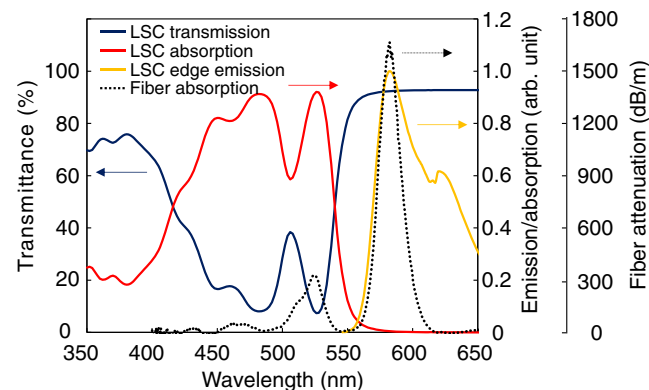

Figure 2. Measured transmittance of the fabricated LSC with its normalized emission/absorption intensities. The measured absorption spectrum of the active fiber, as obtained via the cutback method, is also shown.

Previous theoretical investigations revealed the superiority of enclosing the fiber in the LSC over wrapping it around its edge in the air.[28] To experimentally realize this, an active fiber (length = 50 m) was attached to an ultraviolet (UV)-curable resin (Norland Optical Adhesive, NOA85) at the bottom of the fused silica substrate, as illustrated in Figure 1b,c. n of the optical adhesive was selected to minimize the Fresnel reflections at the interfaces of the fused silica substrate and optical fiber coating resin. An Nd^{3+}-doped aluminosilicate optical fiber (core = 16 μm, numerical aperture (NA) = 0.18; Furukawa Electric Co., Ltd) was employed as the active fiber in this study.[30,31] The coating resin of the fiber was not removed because our preliminary measurements indicated that its effect on light coupling from the LSC into the fiber core was negligible. The smaller diameter (180 vs 300 mm) and the shorter fiber length (50 vs 190 m) of our LSC compared with those of the liquid-state LSC-based SPL were due to the limitations of the fabrication equipment.[27] DM and HRM were added to the front and rear sides of the LSC, respectively, to enhance the confinement of the downshifted photons for pumping the active fiber. The reflection properties of DM and HRM are shown in Figure S1 and S2, Supporting Information. The DM exhibited a cutoff wavelength of 579 nm, which allowed the transmission of a broad range of short-wavelength sunlight into the LSC while preventing the long-wavelength-downshifted photons, which were produced by the luminescent layer, from escaping via the front escape cone of the device.

2.2. Characterization

The small-signal gain ($g_0 l$) is the key performance indicator of SPLs. It was measured by comparing the output power of the probe signal, which was obtained in the lasing wavelength range after passing through the active fiber, with and without the illuminations from the solar simulator. Figure S3a, Supporting Information, shows the scheme of the measurement of the $g_0 l$; Figure S3b, Supporting Information, shows a photograph of the setup during the measurements. The active fiber in the setup is not equipped with an optical feedback mechanism for the $g_0 l$ measurements. The filtered output ($\lambda < 350$ nm and $\lambda > 800$ nm) of the solar simulator (xenon arc lamp, Model Seric XC-500ASS) exhibited an emission spectrum that was close to the visible region of terrestrial sunlight. The collimated output of the solar simulator was adjusted employing a Fresnel lens, as follows: its spot size (beyond the focal point) was adjusted to match the diameter of the LSC. The spectrum of the xenon lamp is plotted in Figure S4, Supporting Information; its total output power, as measured at the focal point employing a laser power meter (Ophir FL250A), was 54 W. This value was applied to calculate the irradiance on the LSC surface (2.1 kW m^{-2}). A superluminescent diode (SLD; Thorlabs, S5 FC), which emitted broadband radiation from 950 to 1170 nm (centered at 1050 nm), was employed as the probe. The output emission power and spectrum of the active fiber were measured by a fiber-coupled near-infrared spectrometer (resolution = 0.65 nm, Ocean Optics NIRQuest 512 1.7). $g_0 l$ was calculated, as follows

$$g_0 l = \ln\left(\frac{T_{\text{pump+probe}}(\lambda) - T_{\text{pump}}(\lambda)}{T_{\text{probe}}(\lambda)}\right) \quad (1)$$

where $T_{\text{pump+probe}}$ and T_{probe} are the measured transmitted spectra of SLD in the fiber with and without xenon-lamp illumination, respectively, and l is the length of the active fiber (50 m). A significant amount of luminescence was produced by the excited Nd^{3+}, thus masking the SLD transmitted signal when the LSC is illuminated by xenon-lamp. This luminescence signal, T_{pump}, was subtracted in the calculations after it was separately measured when SLD was turned off with xenon-lamp illumination.

3. Theoretical Calculations

The theoretical calculations were conducted by a commercially available ray-tracing software, LightTools (Synopsis). The detailed methodology for the simulation, which is similar to that of the previous work, is described in Supporting Information.[28] The wavelengths of the parallel rays, which were emitted from a circular source, were assigned based on the probability distribution of the simulated solar spectrum (Figure S4, Supporting Information), and the incident power was normalized to 2.1 kW m^{-2} (the simulation environment is illustrated in Figure S7a, Supporting Information). The active fiber comprising plastic coating was implemented with multiple toroids; each toroid comprised four layers, as shown in Figure S7b, Supporting Information, thus: the outermost toroid (diameter = 200 μm with $n = 1.51$), the inside of the toroid representing the fiber coating (diameter = 150 μm with $n = 1.48$), the third toroid representing the fiber cladding (diameter = 125 μm with $n = 1.46$), and the inner toroid representing the fiber core (diameter = 16 μm with $n = 1.47$). The three outer layers were assumed to be absorption-free.

4. Results and Discussion

4.1. Measurement of the Differential $g_0 l$

The differential $g_0 l$ was measured at room temperature employing five LSC setups (**Figure 3**). For the LSC1 design, the bare solid-state LSC with the coiled fiber was employed. Regarding LSC2, LSC3, and LSC4, the DM and HRM were placed at the front and rear sides of the LSC, respectively. Therein, the photons, which escaped from the solid-state LSC, were repeatedly reflected between the DM and HRM, thereby enhancing the absorption of Nd^{3+} in the active fiber. Since the LSC was designed to function with HRM, the sufficient absorption of the incident photons from the lamp was achieved by a round trip through the luminescent layer. The absorption through the LSC during a single pass was ≈90% at the peak absorption wavelength (545 nm); it reduced to ≈30% in the UV region (Figure 2, blue line). Regarding LSC3, an n-matching oil ($n = 1.51$) was inserted between the LSC and DM/HRM to disrupt TIR, thereby enabling the reproduction of the liquid LSC by eliminating the air gap between the LSC and DM/HRM. This further clarified the advantages of the solid-state LSC over the liquid-state ones. The reflections of DM and HRM were significantly altered when they contacted the oil (Figure S1 and S2, Supporting Information). To evaluate the amounts of power, which were trapped in the LSC and by the DM/HRM, the
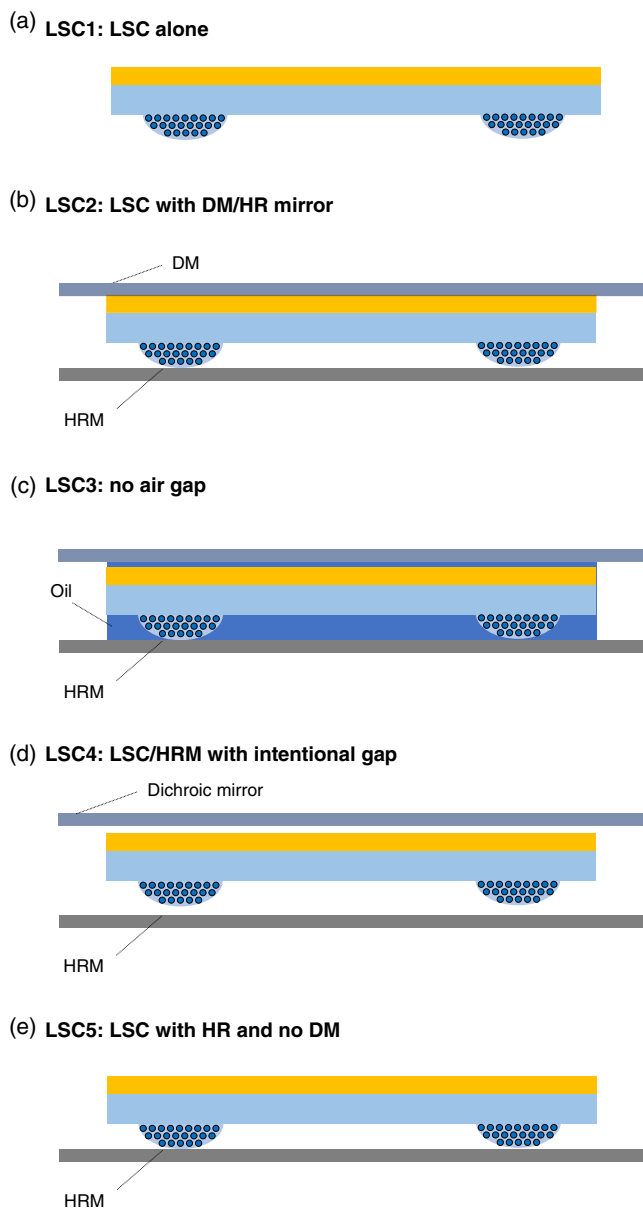
**ADVANCED
SCIENCE NEWS**

www.advancedsciencenews.com

**ADVANCED
PHOTONICS
RESEARCH**

www.adpr-journal.com

(a) **LSC1: LSC alone**

(b) **LSC2: LSC with DM/HR mirror**

DM

HRM

(c) **LSC3: no air gap**

Oil

HRM

(d) **LSC4: LSC/HRM with intentional gap**

Dichroic mirror

HRM

(e) **LSC5: LSC with HR and no DM**

HRM

Figure 3. Five LSC setups (LSC1, LSC2, LSC3, LSC4, and LSC5) for measuring $g_0 l$.

LSC4 configuration was employed for the experiment employing intentional air gaps of different thicknesses between the LSC and mirrors. Compared with LSC4, DM was removed in LSC5 to demonstrate the extreme case involving an infinite gap. The difference between LSC5 and LSC1 was that the former retained the bottom HRM, which facilitated the second pass back of the transmitted photons from the lamp to through the LSC.

The measured $g_0 l$ spectra of LSC1 and LSC2 are displayed in **Figure 4**. The spectra exhibited a very wide bandwidth of 1050–1130 nm, which peaked at ≈1064 nm. The observed spectra were similar to those of the previously observed SPL, which was employed a liquid-state LSC.[27,30] Notably, the shape of the spectrum was independent in the LSC setups. The measured
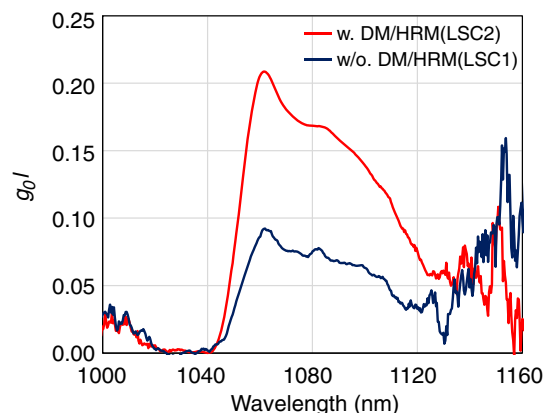

Figure 4. Measured $g_0 l$ spectrum with (LSC2) and without (LSC1) the DM and HRM. The emission wavelength of the superluminescent diode probe (SLD) was 1020–1170 nm.

results revealed that the gain was increased by a factor of 2.2 by sandwiching LSC in DM/HRM.

The results obtained employing LSC1–LSC5 for the measurements are summarized in **Table 1**. When the n-matching oil was inserted into the air gap (LSC3), $g_0 l$ was halved from 0.211 to 0.104. The result indicated that the confinement of the photon by the solid-state LSC (LSC2) was boosted by a factor of 2.1 compared with that by the liquid LSC (LSC3). The results quantitatively verified the advantage of light trapping by combining TIR and the dielectric mirrors, as theoretically predicted.[28]

The luminescence of this proposed solid-state LSC was confined by two different mechanisms. The emission of a photon at an angle that was larger than that, which was required to support TIR at the air/LSC boundary, the photon was repeatedly reflected in the LSC/fiber unit until it was ultimately absorbed. Notably, this discussion neglected the effects of 1) scattering caused by the fiber surface and 2) the non flatness of the surface of the optical adhesive. Conversely, the emission of a photon at an angle that was smaller than the TIR resulted in its escape from the LSC and subsequent reflection by DM or HRM. Since the reflection did not change the angle, the photon generally fluctuated between the DM and HRM at an angle that was smaller than the TIR and was confined in the volume that was defined by these mirrors.

Table 1. Measured $g_0 l$ results employing the five LSC setups (Figure 3).

Setup	Gap distance [mm]	Measured $g_0 l$
LS1	NA	0.095
LS2	NA	0.211
LS3	NA	0.101
LS4	24	0.214
	256	0.203
	537	0.188
	1059	0.165
	2121	0.145
LS5	Infinity	0.108

Although it has been experimentally demonstrated that the photon confinement effect is enhanced by DM/HRM, two questions persist. The first is as follows: because the DM/HRM contacted the LSC, the TIR at the LSC surface, which is assumed to be at the air interface, may be inhibited. The second bothered on the quantitative evaluation of the amounts of trapped power inside the LSC and DM/HRM. The density of the trapped photon between DM and HRM was inversely proportional to the volume between the mirrors, although this volume did not affect the density of the photons in the LSC. Therefore, the ratio of the photon densities in the two regions was evaluated by varying the gap between LSC and the mirrors (Figure 3d and Table 1). Comparing the experimental results with and without the additional small gaps between LSC and the mirrors, the extent of the negative effect of the contact between LSC and DM/HRM could be eliminated.

The measured results demonstrated that the gain decreased as the additional gap distance between DM/HRM increased (Table 1). The decrease was attributed to the lower photon density since the gain reduced inversely to the gap distance. The gain with no intentional gap (LSC2), namely the direct attachment between DM/HRM and the solid-state LSC unit, was almost identical to that of LSC4 exhibiting a very small additional gap (24 µm); this further proved that the tiny air gaps persisted between LSC and the mirrors even when they were directly attached; this is an essential guideline for designing solid-state LSC-based SPL systems.

Depending on the correctness of our interpretation of the mechanism of the confinement of photon density, it should appear, as follows

$$g_0 l = a + \frac{b}{\Delta x + 2000} \tag{2}$$

where a is the gain that was attributed to the energy, which was stored in the LSC; Δx is the additional gap (in µm); and the second term on the right side of the equation represents the gain that was attributed to the energy, which was stored between DM and HRM. The $g_0 l$ factor as a function of the additional gap (red circle) and fitting result to Equation (2) (red line), is plotted in **Figure 5**. The fitting results indicated that a gain of 0.083 out of the total gain (0.211) was stored in the LSC. Put differently, 40% of the total stored energy exist inside the LSC. This small
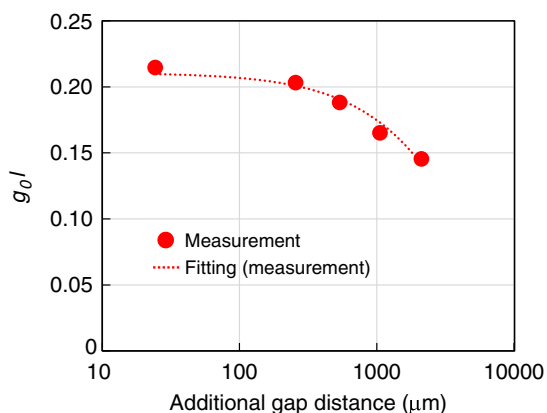
fraction of the energy, which was confined by TIR, correlated with the reported values for dye-topped polycarbonate and polymethyl methacrylate LSCs.[32]

Notably, the edge of the volume, which was subtended by DM and HRM, was open when the experiment was performed. The trapping of more than half of the optical gain obtained from light, which was trapped by the outside of the solid-state LSC, indicated that the addition of an outer edge (to function as a reflector) is effective for enhancing the gain.

4.2. Ray Tracing Simulation

To verify the validity of the model that was described in Section 2, simulations were performed under the same conditions as those of the aforementioned experiments. **Figure 6** shows the comparison between the calculated and experimental results of the gain as a function of the additional gap distance in LSC4. The results further demonstrate that the measured values were well-reproduced via theoretical calculations, indicating that the employed simulation method could be a powerful tool for predicting the performance of the solid-state LSC-based SPLs.

Thereafter, we calculated the extent to which the gain could be enhanced if a toroidal reflector was attached to the volume that was subtended by DM and HRM in LSC2. $g_0 l$ was calculated by adding the reflectivity to the side of the model in Figure S7, Supporting Information, and the results of the $g_0 l$ factor, as a function of the side wall reflectivity, are shown in **Figure 7**. The baseline case was $R = 0$, which matched that of our experimental setup. Figure 7 shows the comparison between the calculated results of the specular and diffuse reflections, indicating that the gain increased from 0.21 to 0.59 after an ideal reflector exhibiting 100% specular reflection was placed as the side wall. Interestingly, the addition of the diffuse reflector afforded almost the same gain as that of the specular reflector. For example, the gain obtained employing the diffuse reflector was 0.46, while that of the specular reflector was 0.49 when they were compared at $R = 0.9$. This finding indicated that it was not necessary to employ complicated and expensive DMs, which were especially challenging to implement on the toroidal surface of the side wall;
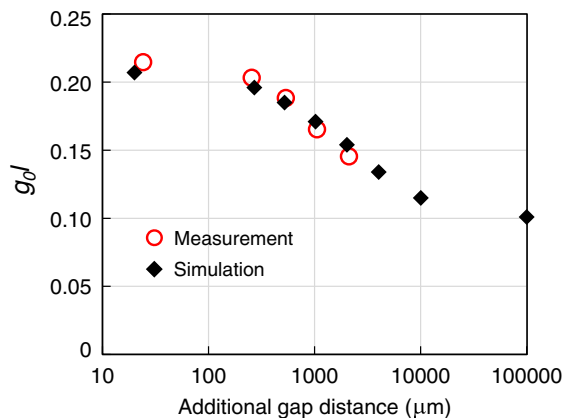
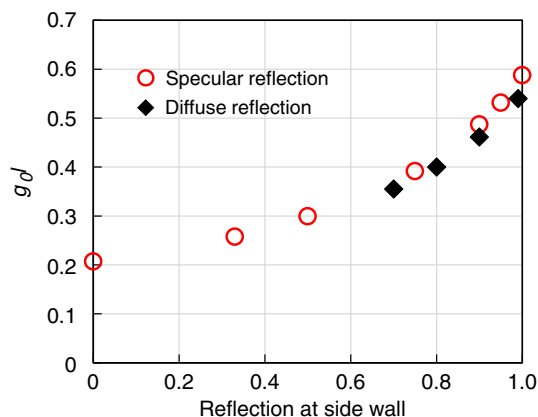**Figure 5.** Measured gain as a function of the additional gap distance.

Figure 6. Measured and simulated $g_0 l$ as a function of the additional gap distance.

Figure 7. Calculated g_0l as a function of the reflectance at the side wall of LSC2.

Figure 9. Measured g_0l spectrum with and without the side-wall reflector (PTFE). The setup without the PTFE ring was the same as LSC2.

this is another crucial guideline for designing solid-state LSC-based SPL systems.

Finally, further experiments were performed to confirm the validity of the predicted enhancement. A ring (width = 8.5 mm), which was produced from polytetrafluoroethylene (PTFE), with a measured reflection of (≈90%) employing diffuse reflection was added to the solid-state LSC as the side-wall reflector. **Figure 8**
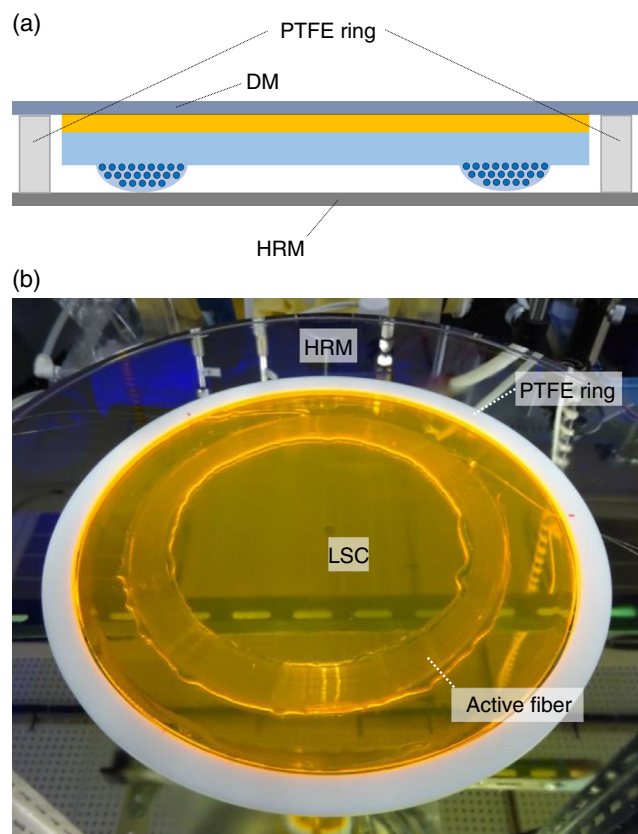

Figure 8. a) Cross-sectional schematic representation and b) photograph of the modified solid-state LSC setup employing the PTFE side-wall reflector.
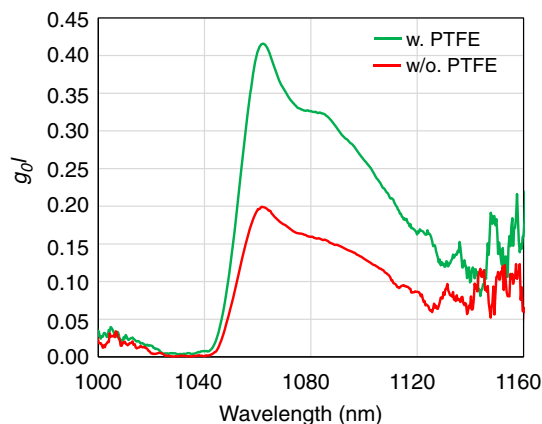
shows the schematic representation and photograph of the modified setup.

The measured g_0l spectra (with and without the side-wall reflector) of LSC2 were plotted (**Figure 9**). The results demonstrated that the measured gain employing the side-wall reflector was 0.42, which was larger by a factor of 1.9 compared with that without the reflector. However, the observed gain (0.42) was slightly smaller than the predicted value (0.46), and this might be attributed to the power leakage at the unintentional small gaps between the PTFE ring and DM/HRM. Thus, this result proved the accuracy of our model, enabling the further investigation of the proposed solid-state LSC-based SPL.

In summary, these results revealed that substituting liquid LSC with the solid-state LSC, which was equipped with a side-wall reflector, resulted in a significant increase in the optical gain in a fully planar SPL. In addition, two beneficial guidelines for practically designing planar SPLs were elucidated: 1) DM and HRM could be directly attached to the solid-state LSC and 2) the reflector exhibiting diffuse reflection instead of a dichroic stack could be applied to SPLs.

5. Conclusions

Five design setups of a thin-film solid-state LSC were investigated to achieve a planar SPL that does not require lens/mirror-based concentration. The theoretical calculations revealed that the optical gain was significantly enhanced by substituting the previous liquid-based LSC design with a solid-state LSC one owing to two reasons: 1) the TIR on the solid-state LSC surface could be explored to improve light confinement and 2) DM/HRM functioned well when a small air gap was maintained between LSC and the mirrors. Afterward, an SPL in which the gain medium (an Nd^{3+}-doped silica optical fiber (length = 50 m) was coiled and adhered to a fused silica disk (diameter = 180 mm), was fabricated employing the solid-state LSC. A thin luminescent layer, which comprised a fluoropolymer film (thickness = 30 μm) containing fluorescent organic dyes (O240 and Y083), was coated on the opposite side of the disk to function as a solid-state LSC. A DM was attached to the dye-coated side, while an HRM was

attached to the fiber side of the LSC. The experimental results demonstrated that the solid-state counterpart exhibited a two-times larger gain compared with the liquid-state LSC in which the sensitizer was held in a volume that was partitioned by the DM/HRM pair, and the active fiber was immersed therein. The numerical calculations indicated that further 2.2-times g_0l enhancement could be achieved by adding a side-wall reflector exhibiting 90% diffuse reflection. This result was experimentally demonstrated, and a 1.9-times enhancement of the optical gain was achieved by applying a PTFE side-wall reflector. Overall, the SPL, which was based on the solid-state design with reflective side walls, exhibited a gain factor of 4.2; this factor is superior to that of its liquid-state predecessor. Although this SPL was equipped with a gain medium, which was only 50 m long owing to the limitations of the fabrication equipment, the model calculations conducted here revealed that the optimum length was two orders of magnitude longer than that of the current setup. Therefore, future works would focus on increasing the fiber length by removing the coating since this would be a key factor for achieving the milestone.

Supporting Information

Supporting Information is available from the Wiley Online Library or from the author.

Conflict of Interest

The authors declare no conflict of interest.

Data Availability Statement

The data that support the findings of this study are available from the corresponding author upon reasonable request.

[1] D. Graham-Rowe, *Nat. Photon.* **2010**, *4*, 64.
[2] Z. J. Kiss, H. R. Lewis, R. C. Duncan Jr., *Appl. Phys. Lett.* **1963**, *2*, 93.
[3] D. Liang, C. R. Vistas, B. D. Tibúrcio, J. Almeida, *Sol. Energ. Mat. Sol. C.* **2018**, *185*, 75.
[4] T. H. Dinh, T. Ohkubo, T. Yabe, H. Kuboyama, *Opt. Lett.* **2012**, *37*, 2670.
[5] S. Mehellou, D. Liang, J. Almeida, R. Bouadjemine, C. R. Vistas, E. Guillot, F. Rehouma, *Sol. Energ.* **2017**, *155*, 1059.
[6] D. Liang, C. R. Vistas, J. Almeida, B. D. Tibúrcio, D. Garcia, *Sol. Energ. Mat. Sol. C.* **2019**, *192*, 147.
[7] D. Liang, J. Almeida, *Appl. Opt.* **2012**, *51*, 6382.
[8] C. J. C. Smyth, S. Mirkhanov, A. H. Quarterman, K. G. Wilcox, *App. Opt.* **2018**, *57*, 4008.
[9] B.D. Tibúrcio, D. Liang, J. Almeida, D. Garcia, C.R. Vistas, P.J. Morais, *Opt. Commun.* **2020**, *460*, 125156.
[10] T. Hisatomi, K. Domen, *Nat. Catal.* **2019**, *2*, 387.
[11] I. Levchenko, K. Bazaka, S. Mazouffre, S. Xu, *Nat. Photon.* **2018**, *12*, 649.
[12] Editorial, *Nat. Mater,* **2018**, *17*, 845.
[13] Y. Zhao, Y. Sun, Y. He, S. Yu, J. Dong, *Sci. Rep.* **2016**, *6*, 38044.
[14] Y. Takeda, H. Iizuka, S. Mizuno, K. Hasegawa, T. Ichikawa, H. Ito, T. Kajino, A. Ichiki, T. Motohiro, *J. Appl. Phys.* **2014**, *116*, 014501.
[15] D. Goto, H. Yoshida, H. Suzuki, K. Kisara, K. Ohashi, presented at *Int. Conf. on Space Optical Systems and Applications (ICSOS)*, National Institute of Information and Communications Technology Vol. S5-2, **2014**.
[16] L. Torres-Soto, L. Summerer, *Proc. of the 59th IAC.*, International Astronautical Federation (IAF) **2008**, IAC-08-C, 3.1.2.
[17] Z. Guan, C. M. Zhao, S. H. Yang, Y. Wang, J. Y. Ke, H. Y. Zhang, *Laser Phys. Lett.* **2017**, *14*, 055804.
[18] T. Yabe, S. Uchida, K. Ikuta, K. Yoshida, C. Baasandash, M. S. Mohamed, *App. Phys. Lett.* **2006**, *89*, 261107.
[19] M. S. Mohamed, T. Yabe, C. Baasandash, Y. Sato, Y. Mori, L. Shi-Hua, *J. Appl. Phys.* **2008**, *104*, 113110.
[20] H. Costa, J. Almeida, D. Liang, D. Garcia, M. Catela, B. D. Tibúrcio, *Opt. Eng.* **2020**, *59*, 086103.
[21] W. Nsengiyumva, S. GuoChen, L. Hu, X. Chen, *Renew. Sust. Energ. Rev.* **2018**, *81*, 250.
[22] G. S. A. Solargis s.r.o., https://globalsolaratlas.info/map, (accessed: June 2021).
[23] R. M. Swanson, *Prog. Photovolt.* **2000**, *8*, 93.
[24] K. Jin, W. Zhou, *IEEE T. Power Electr.* **2019**, *34*, 3842.
[25] T. Motohiro, Y. Takeda, H. Ito, K. Hasegawa, A. Ikesue, T. Ichikawa, *Jpn. J. Appl Phys.* **2017**, *56*, 08MA07-1 - 08MA07-6.
[26] C. B. Roxlo, E. Yablonovitch, *Opt. Lett.* **1983**, *8*, 271.
[27] T. Masuda, M. Iyoda, Y. Yasumatsu, S. Dottermusch, I. A. Howard, B. S. Richards, *Commun. Phys.* **2020**, *3*, s42005-020-0326-2.
[28] S. Dottermusch, T. Masuda, M. Endo, B. S. Richards, I. A. Howard, *Adv. Opt. Mater.* **2021**, *9*, 2100479.
[29] T. Masuda, Y. Zhang, C. Ding, F. Liu, K. Sasaki, Q. Shen, *J. Appl. Phys.* **2020**, *127*, 243104.
[30] T. Masuda, M. Iyoda, Y. Yasumatsu, M. Endo, *Opt. Lett.* **2017**, *42*, 3427.
[31] J. F. Bisson, M. Iyoda, Y. Yasumatsu, M. Endo, T. Masuda, *J. Opt. Soc. Am. B.* **2019**, *36*, 736.
[32] M. G. Debije, P. P. C. Verbunt, B. C. Rowan, B. S. Richards, T. L. Hoeks, *Appl. Opt.* **2008**, *47*, 6763.